Polym. Bull. (2012) 68:1641–1661
DOI 10.1007/s00289-011-0659-9

ORIGINAL PAPER

Electrical conductivity and optical properties of a new quaternized polysulfone

Luminita-Ioana Buruiana · Ecaterina Avram · Adriana Popa · Valentina Elena Musteata · Silvia Ioan

Received: 6 September 2011 / Revised: 14 October 2011 / Accepted: 17 October 2011 /
Published online: 27 October 2011

Abstract Quaternized polysulfone with triphenylphosphonium pendant groups was investigated, as to its optical and electronic properties. Optical properties were analyzed by refractivity and transmission spectra. To obtain the optical parameters, the approach proposed by Tauc for amorphous semiconductors has been used, because of the similarity of the absorption edges. Values of pseudogap energy and Urbach energy of 3.89 eV and 168 meV, respectively, were obtained. The dielectric properties and AC-conductivity were also studied as a function of temperature and frequency. Decrease in the dielectric constant was observed with the increase in frequency and decrease in temperature. Also, quaternized polysulfone films were characterized by two relaxation processes, γ and β relaxation, which appear at different temperatures, depending on the pendant group. The frequency–temperature-dependent conductivity showed that conductivity increases with frequency and also that the quaternized polysulfones possess typical semiconducting properties. All parameters have been found as slightly influenced by the polymer chain structure.

Keywords Quaternized polysulfone · Optical properties · Dielectric properties · Electrical conductivity

Introduction

Polysulfone (PSF) is one of the most attractive polymeric materials used in the manufacture of synthetic polymer membranes and also in biomedical fields, due to

L.-I. Buruiana · E. Avram · V. E. Musteata · S. Ioan (✉)
"Petru Poni" Institute of Macromolecular Chemistry, 41A Gr. Ghica Voda Alley,
700487 Iasi, Romania
e-mail: ioan_silvia@yahoo.com

A. Popa
Institute of Chemistry Timisoara of Romanian Academy, 24 Mihai Viteazu Blv.,
300223 Timisoara, Romania

its excellent properties, such as mechanical, thermal and chemical stability, as well as to its excellent film-forming properties [1, 2]. Also, polysulfones exhibit the unique advantage of transparency, coupled with hydrolytic stability and heat resistance that makes them useful as covers and lids for hot serving dishes and containers, lids for medical sterilization trays, research lab animal cages, dairy processing equipment, flow meters, and sight glasses for chemical process equipment [3]. Also, PSF membranes possess the highest biocompatibility among all types of membranes [4]. Different configurations of the PSF membranes are used as flat sheets or hollow fibers, primarily for microfiltration, and ultrafiltration separation applications [5, 6]. Their main disadvantage is related to the relatively hydrophobic character of PSF. For this reason, researches are now focusing on the synthesis of new polymers that match to desired applications. Modification procedures allow a compromise between hydrophobicity and hydrophilicity; in this way, the modified membranes combine the superior bulk properties of the hydrophobic polymers with the good surface characteristics of the hydrophilic ones [7].

Incorporation of desirable hydrophilic functionalities onto PSF can be accomplished via plasma treatment [8, 9], ultraviolet irradiation, chemical reaction of hydrophilic components onto PSF [10–13], and hydrophilic polymer coating and blending [14, 15]. Modified polysulfones exhibit attractive properties, which recommend them for a wide range of industrial, environmental, electronic, and biomedical applications [16–19].

Among the reactive groups, the chloromethyl one is especially useful, because it can be readily modified by a substitution reaction. Therefore, polymers with chloromethyl pendant groups are often used as starting materials for obtaining new functional polymers [20] with hydrophilic groups (e.g., hydroxyl, amine, carboxyl, and sulfone) grafted onto the backbone chain polymer. Synthesis of phosphonium salts bonded to macromolecular supports has been discussed in detail, due to their numerous applications as phase-transfer catalysts, polymeric reagents for Witting reactions, polycationic biocides [21, 22].

On the other hand, the search for alternative proton-conducting membranes capable of operating at high temperatures has extended the focus of the research area, and increased the interest for investigating alternative phosphonic "protogenic" groups which have the ability to facilitate proton conductivity under low-humidity conditions [23–26]. Thus, polymers carrying these groups have properties quite different from those of polysulfones. For example, phosphonated polymers generally show a higher degree of hydrogen bonding and a lower water uptake, comparatively with their sulfonated compounds. Moreover, phosphonated model compounds have been recently shown to possess an attractive combination of properties that further motivates investigation of phosphonated polymers as proton conductors under low-humidity conditions [23]. Since this is a relatively new topic, some key characteristics of the phosphonic units, have to be underlined as compared to the sulfonic units.

According to our recent work [27], modification of polymers with aromatic structure-bearing chloromethyl groups with a phosphorus reactive compound induces some differences, in comparison with the aliphatic structures (i.e., differences of

reactivity, influence of the substitution degree, etc.). The results showed a high hydrophobicity of phosphorus-modified polysulfones [28] in which the work of spreading of water takes high negative values, and the work of water adhesion is very low in comparison with the work of water cohesion. Also, the investigation evidenced the influence of the substitution degrees on surface characteristics. At the same time, studies of dielectric spectra at different temperatures revealed that the dielectric constant of these polymers increased at higher substitution degrees, as a result of the competition between the main chain and pendant group contributions [29].

The aim of this study is to investigate the optical characteristics, the electrical and conduction properties of a new quaternized polysulfone with triphenylphosphonium pendant groups, over a large domain of frequencies and temperatures.

Experimental

Materials

UDEL-1700 polysulfone (Union Carbide) (PSF) ($M_n = 39000$ g/mol; $M_w/M_n = 1.625$), a commercial product, was purified by repeated reprecipitations from chloroform and dried for 24 h in vacuum, at 40 °C, before being used in the synthesis of chloromethylated polysulfone. A mixture of commercial paraformaldehyde with an equimolar amount of chlorotrimethylsilane (Me_3SiCl) as a chloromethylation agent, and stannic tetrachloride ($SnCl_4$) as a catalyst, was used for the chloromethylation reaction of polysulfone, at 50 °C. The reaction time necessary to obtain chloromethylated polysulfones (CMPSF) was 72 h. Finally, the samples were dried under vacuum at 40 °C.

Polysulfone with triphenylphosphonium pendant groups, PSFP, was synthesized by reacting chloromethylated polysulfone (6.29% chlorine content) with triphenylphosphine. The quaternization reaction was performed by mixing of CMPSF (6.29% chlorine) with triphenylphosphine (PPh_3) in the presence of dioxane. The mixture was maintained under stirring, in nitrogen atmosphere, for 15 h at 90 °C. The viscous product thus obtained was filtered, washed with dioxane and ethylether, and finally dried. The contents of ionic chlorine, Cl_i, and total chlorine, Cl_t, were determined by potentiometric titration (Titrator TTT1C Copenhagen), with 0.02 N $AgNO_3$ aqueous solutions. The ratios between the ionic chlorine and total chlorine contents show that the quaternization reaction of CMPSF occurs with about 46% transformation degree.

The general chemical structures of the studied polysulfones (PSF, CMPSF and PSFP) are presented in Scheme 1.

Table 1 lists the structural characteristics of the polysulfone with triphenylphosphonium pendant groups and Fig. 1 shows ATR-FT-IR spectrum (recorded on film, using a Nicolet-6700 ATR-FT-IR spectrometer (Thermo Electro Corporation), in the range 400–4000 cm^{-1}) which proves the structure of PSFP. The infrared spectrum shows two characteristic absorption peaks at 3060–3200 cm^{-1} and 1665–2000 cm^{-1}, which refers to bands characteristic to aromatic rings. In addition, the band at 1294 cm^{-1} is attributed to SO_2 group and the vibrational band observed

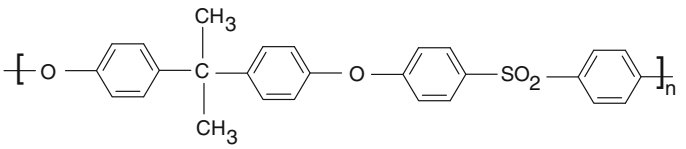

PSF

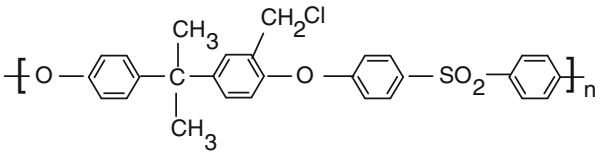

CMPSF

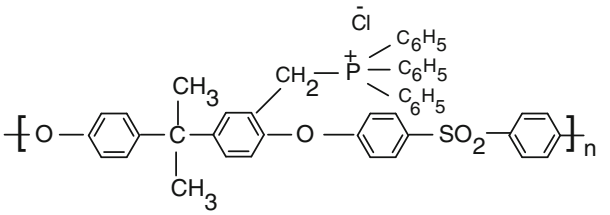

PSFP

Scheme 1 General structure of different polysulfones

Table 1 Total chlorine, Cl_t, ionic chlorine, Cl_i, substitution degree, phosphorus content, P, and functionalization degree of polysulfone with triphenylphosphonium pendant groups

Sample	Cl_t (%)	Cl_i (%)	Substitution degree	P (%)	Functionalization degree (mmol phosphonium groups/g polymer)
PSFP	4.43	2.06	0.46	2.40	0.773

at 2854–2965 cm^{-1} is associated with C–H stretching from alkyl groups (–CH, $–CH_2$, $–CH_3$). The band at 1150–1169 cm^{-1} is assigned for $–P–CH_2–$ bond, while the absorption corresponding to P-aryl stretching occurs at 1047–1082 cm^{-1}. A band characteristic to triphenylphosphonium salts can be observed at 1105 cm^{-1}.

Also, Fig. 2 shows 2D and 3D AFM images of PSFP film surface prepared by solution in *N*,*N*-dimethylformamide (DMF) drop casting on glass slide. The scanning area of 5×5 μm^2 reveals porous morphology, with various pore sizes (pore diameter ranging between 39 and 471 nm) and two- or three-dimensional ordered structures. These pores were naturally formed during the evaporation of the solvent. The value of 5.16 nm for root mean square (RMS) roughness obtained by analyzing topography image was influenced by the pores presence. AFM images were obtained on a SPM SOLVER Pro-M instrument. A NSG10/Au Silicon tip with a 10 nm curvature radius and 286 kHz oscillation mean frequency.

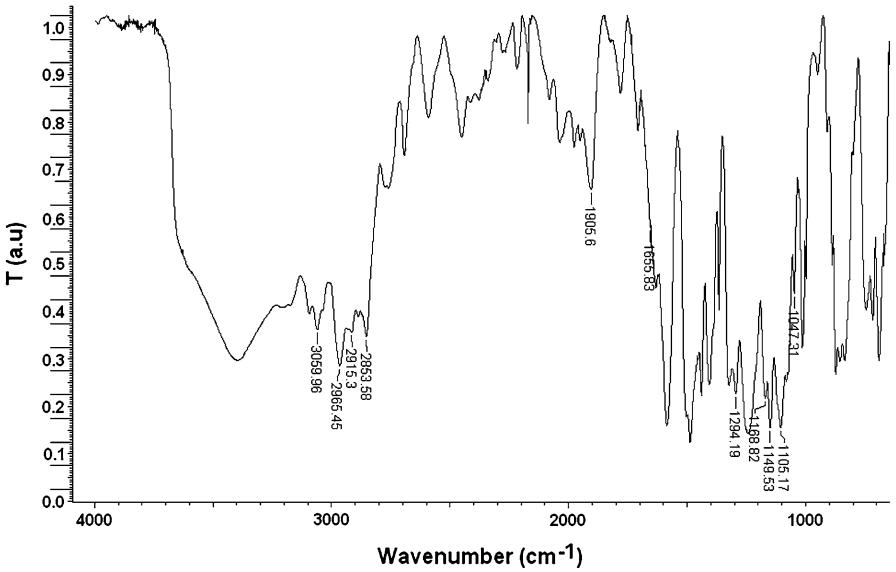

Fig. 1 ATR-FT-IR spectra for PSFP in 4000–400 cm^{-1} spectral regions

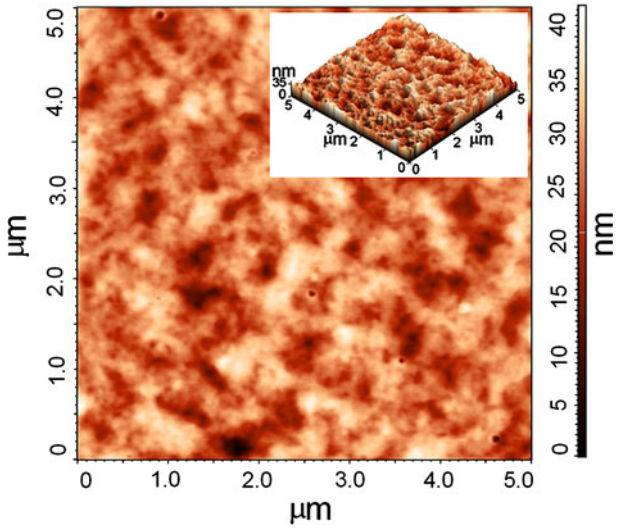

Fig. 2 2D and 3D AFM images of PSFP film, for 5 × 5 μm^2 scan area

Optical investigations

The refractive indices of the polysulfone with triphenylphosphonium pendant groups, *n*, were measured both experimentally, with an Abbé refractometer at 25 °C, and theoretically, using Eq. 1 proposed by Lorenz [30] and Lorentz [31]:

$$R_u = V_u x(n^2 - 1)/(n^2 + 2) \quad (1)$$

where n is the refractive index, and V_u and R_u are the molar volume and molar refractivity, respectively, of quaternized polysulfone, expressed in Eqs. 2 and 3:

$$V_u = \sum_i a_i \times V_i \quad (2)$$

$$R_u = \sum_i a_i \times R_i \quad (3)$$

where V_i and R_i are the contributions of molar volume and molar refractivity, respectively, corresponding to particular functional groups within the polymer repeating unit, and a_i is the number of i groups from the repeating unit.

Transmittance of the polysulfone here under study was recorded at 200–1100 nm wavelengths, on a SPECORD 200 Analitik-Jena spectrophotometer. The films were prepared from PSFP solutions with 5 g/dL concentration, in DMF. The polymer solutions were cast on a glass plate and solidified initially by slow drying in saturated atmosphere of the used solvents, and finally under vacuum, at 35 °C. The polysulfone with triphenylphosphonium pendant groups films thus prepared were subjected to transmittance and conductivity investigations.

Dielectric and conductivity measurements

Dielectric spectroscopy (DS) measurements over the 10^0 to 10^6 Hz frequency range were carried out using a Novocontrol Concept 40 broadband dielectric spectrometer. Temperature was controlled with a 0.1 °C device by the Novocontrol Quatro Cryosystem, in dry nitrogen atmosphere. The sample was sandwiched between two gold-coated brass electrodes and tested. The sample had around 2 mm thickness, with slightly larger diameters than those of the upper electrode (20 mm).

Dielectric measurements (dielectric constant, ε', and dielectric loss, ε'') and AC-conductivity of PSFP films, prepared from solutions in DMF, were performed by sweeping the frequency between 10^0 and 10^6 Hz, at fixed temperatures, at 4 °C intervals, over a temperature domain between −150 and +120 °C, at an increasing temperature rate of 2 °C/min.

Results and discussion

Optical properties

Typical transmission spectra of the investigated polysulfone with triphenylphosphonium pendant groups films prepared from solutions in DMF over the whole measured range of 200–1200 nm wavelengths are shown in Fig. 3. The transmission spectra, initiated in the ultraviolet domain, present a value of about 85% transparency for films prepared in DMF.

To obtain the absorption coefficient, α, from transmittance data, Eq. 4 was used:

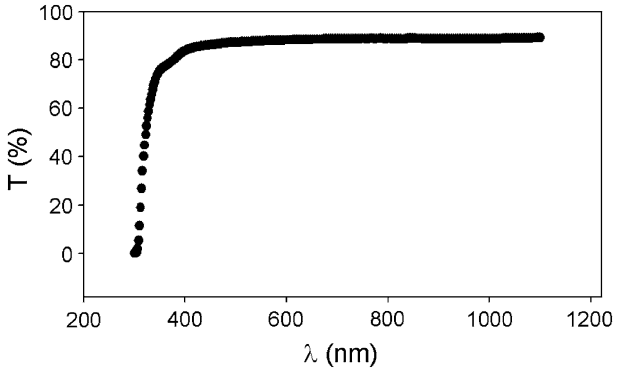

Fig. 3 Typical overall transmission spectra of polysulfones with triphenylphosphonium pendant groups films prepared from solutions in DMF

$$\alpha = (1/d)\ln(1/\text{transmittance}) \tag{4}$$

where d is film thickness.

Generally, for a typical amorphous semiconductor, three domains are evident in the variation of the absorption coefficient versus photon energy:

- in the first region, the absorption coefficient due to inter-band transition near the band gap describes the optical gap energy E_G in amorphous semiconductors;
- in the second region, absorption at photon energy below the optical gap depends exponentially on photon energy, which defines the Urbach edge energy, E_U. The theories of the Urbach edge are based on the idea that the sharp absorption edge is broadened by some kind of mechanism. For example, in semiconductors, the exponential edges are due to the electric fields produced by charged impurities. Besides the charged impurities, there are also other possible sources of internal electric fields. One of them is represented by density fluctuations via the piezoelectric effect in semiconductors with a piezoelectric constant different from zero. In amorphous materials, such density fluctuations do not change with time, so that the exponential edge can be thought of as due to frozen-in longitudinal optical phonons;
- the third region describes the optical absorption generated by defects appearing at an energy lower than the optical gap. This energy, E_T, the so-called Urbach tail, refers to the weak absorption tail and describes the defect states; this energy is rather sensitive to the structural properties of the materials. This absorption tail lies below the exponential part of the absorption edge (the second region), and its strength and shape were found to depend on the preparation, purity and thermal history of the material, varying only slightly with its thickness.

From the obtained data, the absorption coefficient was plotted in Fig. 4 for the studied film, as a function of photon energy, according to Eq. 5:

$$\alpha = \alpha_0 \exp(E/A) \tag{5}$$

where α_0 is a constant and E is photon energy.

The shape of the curve is very similar to the behavior proposed by Tauc for a typical amorphous semiconductor [32–34], although the absorption level is lower than for amorphous, inorganic thin films. These results agree with other literature data, which assume that a lower absorption in polymer materials is due to a lower degree of bonding delocalization [35, 36]. An absorption edge is a sharp discontinuity in the absorption spectrum by an element that occurs when the energy of the photon corresponds to the energy an atom shell. Each of the absorption edges in Fig. 2 exhibits two different slopes, and a saturation region for higher energy. Parameter A becomes either E_U, in the high-energy region, or E_T in the low-energy region of the absorption coefficient.

For the investigated sample, the absorption edges were found to follow the Tauc power law (Eq. 6) in the range over which photon energy was higher than optical gap energy, E_G:

$$(\alpha \cdot E)^{1/2} = B(E - E_G) \tag{6}$$

where B is a constant.

Thus, the dependencies plotted in Fig. 5 were used to obtain the Tauc optical gap energy, E_G, for PSFP. The approach, typical for amorphous semiconductors, has been also applied to polymer films [37]. The values of the obtained optical parameters illustrated in Figs. 4 and 5 are listed in Table 2. One can observe that these parameters possess sensitive properties which may be influenced by many different factors, such as, for example, the conditions of films preparation from solution, where air oxidation or the dissolving power of the DMF lead to changes in film transmittance. Thus, the energy gap E_G values exceeded 3.26 eV for transparent films prepared in DMF. Studies were compared with the modified polysulfones PSF-DMEA and PSF-DMOA, obtained by the quaternization reaction of chloromethylated polysulfones with *N*-dimethylethylamine and *N*-dimethyloctylamine, respectively [38].

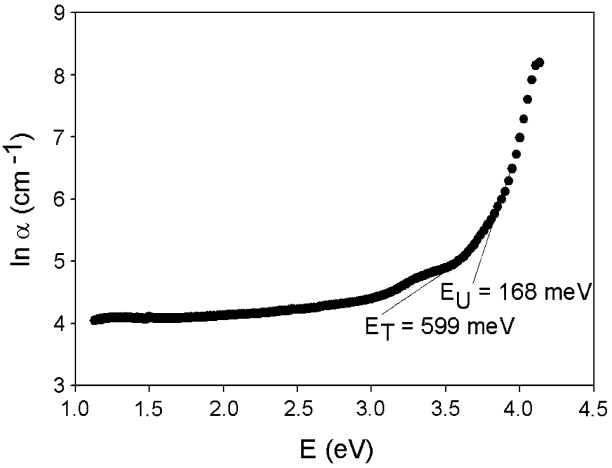

Fig. 4 Absorption coefficients of polysulfone with triphenylphosphonium pendant groups, with films prepared from solution in DMF. The values of E_U and E_T were obtained from the lines slopes from figure

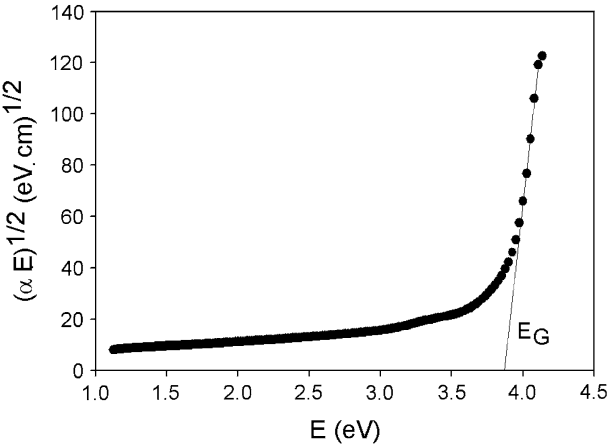

Fig. 5 Tauc dependence of polysulfone with triphenylphosphonium pendant groups with films prepared from solution in DMF

Table 2 Optical parameters of polysulfone with triphenylphosphonium pendant groups films, prepared in *N*,*N*-dimethylformamide solution

Sample in DMF	d (μm)	E_T (meV)	E_U (meV)	E_G (eV)
PSFP	20	599	168	3.89
PSF-DMEA [38]	10	1657	157	3.62
PSF-DMOA [38]	20	1308	165	3.61

The history of films preparation also influenced E_U and E_T values. The value of Urbach energy was 168 meV, which agrees with the specific values for transparent polymers. Also, the E_T energy for transparent polysulfone has a low value (599 meV). These two parameters are related to the localized state induced by the polymer atomic structures. Possible structural defects, such as breaks, configurational imperfections, or torsions of the polymer chains, seem to be responsible for the energy described by Urbach tail energy, E_T. Moreover, larger structural disorder and charged impurities may cause an increase in Urbach energy, E_U. In this context, our data show that E_U and E_T are specific for films obtained from transparent polymer solutions. One can observe that gap energy and the electric fields produced by charged impurities—expressed by Urbach edge energy—have approximately the same values with previous data obtained for PSF-DMEA and PSF-DMOA quaternized polysulfones, but the defect states expressed by Urbach tail energy have lower values than for PSF-DMEA and PSF-DMOA; this could be attributed to the different structure of triphenylphosphonium, *N*-dimethylethylammonium, or *N*-dimethyloctylammonium from the side groups.

Dielectric properties

The dielectric constant depends on both chemical structure and polarization mechanisms. Dielectric constant magnitude or the refractive index, depending on

the ability of the polarizable units from the polymer structure to orient them fast enough to keep up with the oscillations of an alternating electric field, is characterized by the dipole moment per unit volume induced by the electromagnetic field. At optical frequencies (approximately 10^{15} Hz), only the electrons—the lowest mass species—are efficiently polarized. At lower frequencies, atomic polarization of the nuclei, which move more slowly than the electrons, contributes to the dielectric constant, too. Contribution of each polarization mode to the dielectric constant is expressed in Eq. 7 [39]:

$$\varepsilon = \varepsilon_{\text{electronic}} + \varepsilon_{\text{atomic}} + \varepsilon_{\text{dipolar}} \tag{7}$$

where $\varepsilon_{\text{electronic}}$ is the dielectric constant corresponding to electronic polarization at optical frequencies (10^{15} Hz); $\varepsilon_{\text{atomic}}$ is the dielectric constant corresponding to atomic polarization at lower frequencies (10^{12} Hz); $\varepsilon_{\text{dipolar}}$ is the dielectric constant corresponding to dipolar polarization occurring at microwave (10^{9} Hz). In solid state, alignment of the permanent dipoles requires considerably more time than electronic or atomic polarization, occurring at microwave (10^{9} Hz) or at much lower frequencies. At optical frequencies around 10^{15} Hz, only the electrons are efficiently polarized. Under these conditions, the dielectric constant, $\varepsilon_{\text{electronic}}$, can be determined with Maxwell relationship, which assumes knowledge of the refractive indices, n, according to Eq. 8 [39]:

$$\varepsilon_{\text{electronic}} = n^2 \tag{8}$$

Thus, a theoretical study was performed to calculate the refractive index and, implicitly, the $\varepsilon_{\text{electronic}}$ of PSFP from the contribution of the individual atoms, according to Eq. 1, in which molar refraction, R_u, and molar volume, V_u, were calculated with Eqs. 2 and 3, while the contributions of various substructures, R_i and V_i, were taken from literature (Table 3) [40, 41]. The R_u, V_u, and n results are illustrated in Table 4. The theoretical values of the refractive index correspond to transparent materials. Also, these data are close to our experimental evaluations.

Table 3 Increments of various R_i and V_i substructures [40]

Increment	R_i (cm^3/mol)	V_i (cm^3/mol)	R_i/V_i
–CH_2–	4.504	15.528	0.290
p-C_6H_4 (aromatic)	25.235	65.912	0.383
–CH_3	5.901	25.798	0.229
C_6H_3 (aromatic)	24.785	53.710	0.462
>SO_2	9.630	27.713	0.348
–O– (ether)	1.625	9.052	0.180
P [41]	7.970	17.000	0.469
–C–CH_3	7.875	22.645	0.347
CCl_3	20.620	67.096	0.307
CCl_2	15.786	41.498	0.380
C_6H_5 (aromatic)	25.824	74.129	0.348

Table 4 Molar refraction, R_u, molar volume, V_u, theoretical, n_{th}, and experimental, n_{exp}, values of the refractive index, n, and dielectric constant, $\varepsilon_{electronic}$, for PSFP

Sample	R_u (cm^3/mol)	V_u (cm^3/mol)	R_u/V_u	n_{th}	n_{exp}	$\varepsilon_{electronic}$
PSFP	221.944	663.541	0.334	1.584	1.580	2.509
					1.585*	2.512[a]

[a] Data obtained from extrapolation of the dielectric constant versus frequency, at optical frequency (10^{15} Hz) (see Fig. 7)

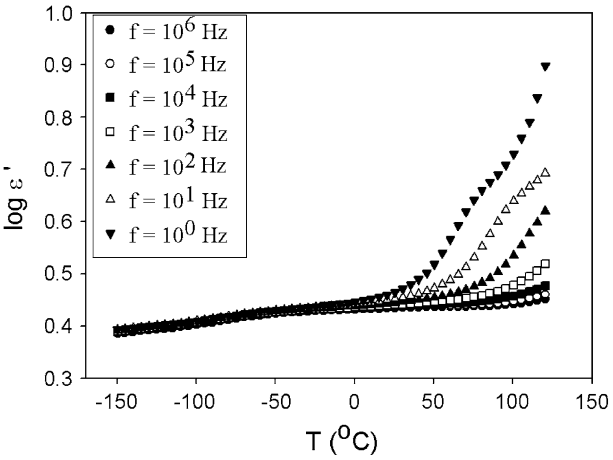

Fig. 6 Logarithmic plot of the dielectric constant versus temperature at different frequencies, for PSFP

AC-dielectric measurements at different frequencies and temperatures

A dielectric study was developed for PSFP in DMF, in the frequency range from 1 Hz to 10^6 Hz, and temperature range between −150 and +120 °C. Figure 6 presents the dielectric constant (i.e., permittivity) (ε') as a function of temperature, at different frequencies.

The dielectric constants increased with temperature, due to the increase of total polarization, arising from dipoles orientation and trapped charge carriers, and decreased with increasing frequency, due to dielectric dispersion, as a result of the lag of molecules behind the alternation of the electric field at higher frequency [42]. One can observe that, for the studied sample, the dielectric constant depends on the main chain and on the pendant group. On the other hand, the pendant groups reduced the electronic conjugation from the main chain and resulted in lower values of ε', comparatively with the unmodified polysulfone. In this context, Saxena et al. [43] found out, from the PSF dielectric spectrum at 30 °C, ε' values of 4.3 at 100 Hz and 3.7 at 500 Hz. Moreover, triphenylphosphonium from the side groups reduces more the electronic conjugation from the main chain, lower values of ε' and lower slopes of log ε' versus temperature thus resulting, comparatively with the quaternized polysulfones with *N*-dimethylethylammonium or *N*-dimethyloctylammonium side groups [38].

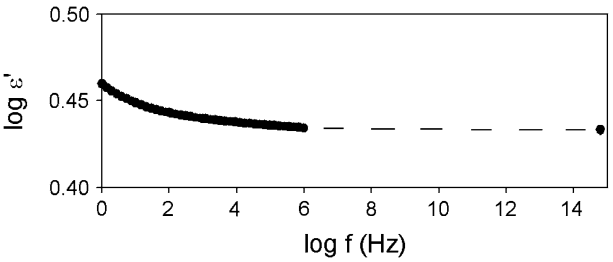

Fig. 7 Double logarithmic plot of the dielectric constant versus frequency at 20 °C, for PSFP

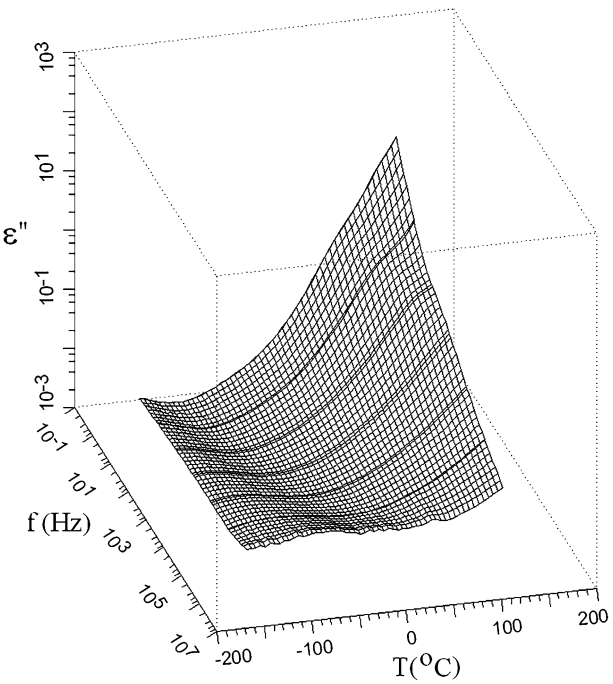

Fig. 8 Frequency and temperature dependencies of the dielectric loss for PSFP

The experimental and theoretical results obtained for the refractive index and the corresponding values of dielectric constants (obtained from Maxwell's equation) were consistent with the values obtained in Fig. 7, by extrapolating the dielectric constant versus frequency to optical frequency (10^{15} Hz) (see Table 3).

Variation of dielectric loss with frequency and temperature

Figure 8 exhibits the tridimensional variation of dielectric loss, ε'', with frequency and temperature, for the studied sample. One can observe that the main contribution to dielectric relaxation appears in the frequency range attributed to the motion of

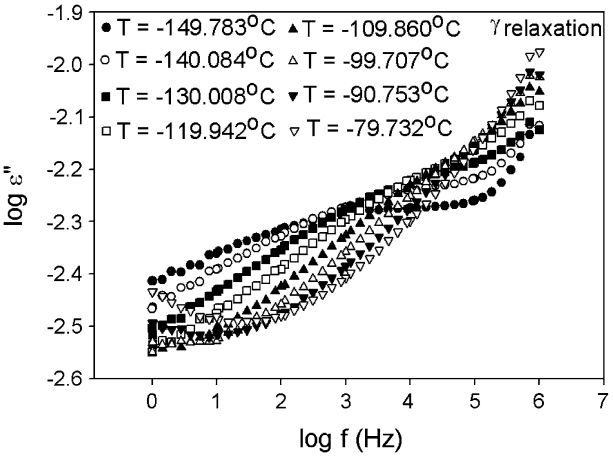

Fig. 9 Dielectric loss versus frequency for PSFP in the frequency domain of γ relaxation

the side groups. Thus, in the dielectric relaxation spectrum between -150 and $+120$ °C, γ relaxation is observed at very low temperatures, in the $-145 \div -100$ °C range, for different frequencies. This process is called secondary or local relaxation. Detailed spectrum results for γ relaxation are shown in Fig. 9, which presents dielectric loss versus frequency for the PSFP sample in the frequency domain of γ relaxation. On the other hand, β relaxation appears very weak at 70 °C, at high frequencies, and becomes indistinguishable at lower frequencies, so that the activation energy could not be determined.

Unlike quaternized polysulfones, polysulfone films are characterized by two transition temperatures, i.e., β transition at approximately 75 °C, caused by the micro-Brownian motion of the main chain segments—due to the flexibility of their molecules—and α transition at 197 °C, caused by a rotatory diffusional motion of the molecules from one quasi-stable position to another one, around the skeletal bond, involving large-scale conformational rearrangement of the main chain [43]. α relaxation does not appear in quaternized polysulfones because of the losses caused by increased conductivity. In addition, the thermal decomposition temperatures of quaternized polysulfones do not exceed 150 °C, while that of polysulfone is approximately 400 °C [44].

The relaxation time for γ relaxation, τ_{max}, which is correlated with the maximum frequency for dielectric relaxation by the $f_{max} = (2\pi\tau_{max})^{-1}$ dependence, is plotted versus the reciprocal temperature (i.e., Arrhenius plots) in Fig. 10, for the $-145 \div -100$ °C temperature range. The obtained value for activation energy, E_a, is 0.202 eV.

Literature [45] shows that, in the sub-glass relaxation domain, the activation energy associated with each relaxation is related to the relaxation temperature and to its corresponding activation entropy at a frequency of 1 Hz, according to the approach described by Starkweather [46, 47]. The local-mode γ relaxation of the main chain appears to involve a spectrum of motions in which the limiting low-temperature, high-frequency component has an activation entropy close to zero.

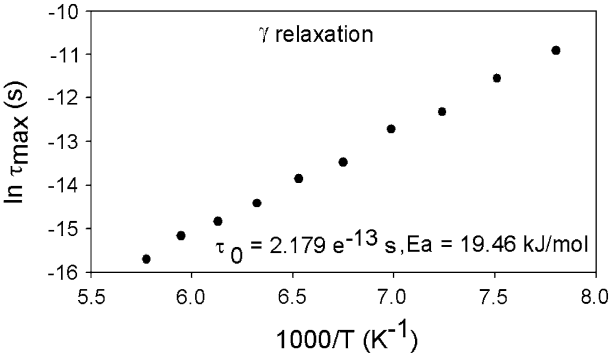

Fig. 10 T_{max} from dielectric loss versus temperature (i.e., Arrhenius plots) for γ relaxation determined for PSFP

Taking into consideration that the strength and frequency of relaxation depend on the characteristic properties of dipolar and ionic relaxation, the present study can also provide some information on the modification of local relaxation [48]. Thus, individual relaxations can be described using the Havriliak-Negami (HN) expression:

$$e* = \varepsilon' - i\varepsilon'' = \varepsilon_U + \frac{\varepsilon_R - \varepsilon_U}{\left[1 + (i\omega\tau_{HN})^a\right]^b} \tag{9}$$

where ε_R and ε_U represent the relaxed ($\omega \to 0$) and unrelaxed ($\omega \to \infty$) values of the dielectric constant for each relaxation, $\omega = 2\pi f$ is the frequency, τ_{HN} is the relaxation time for each process, and a and b represent the broadening and skewing parameters, respectively [49]. When parameter a is much below 1, the distribution of the relaxation time is broader. Also, when parameter b is equal or smaller than 1, dielectric dispersion is symmetrical or asymmetrical, respectively. In the case of γ relaxation, occurring at very low, negative temperatures, the mean values are $a \cong 0.287$ and $b \cong 1$ for the PSFP sample, evidencing a relatively broad distribution of the relaxation times and a symmetrical dielectric dispersion. The relaxation intensity, $\Delta\varepsilon = \varepsilon_R - \varepsilon_U$, corresponding to the PSFP sample for γ relaxation, changes with temperature (8.39×10^{-2} to 8.84×10^{-2} in $-145 \div -100$ °C range), reflecting an apparent loss of the net dipolar correlation with thermal energy increasing [45].

Electrical modulus analysis

Conductivity behavior in the frequency domain is more conveniently interpreted in terms of conductivity relaxation time, τ, using the representation of electrical modulus, $M^* = 1/\varepsilon^*$. The M*representation is now widely used to analyze ionic conductivities, by associating a conductivity relaxation time with the ionic process [50]. Thus, the electric modulus M*is defined in terms of the reciprocal of the complex relative permittivity, ε* (Eq. 10):

$$M^* = \frac{1}{\varepsilon^*} = M' + iM'' \tag{10}$$

where $M' = \frac{\varepsilon'}{\varepsilon'^2 + \varepsilon''^2}$ and $M'' = \frac{\varepsilon''}{\varepsilon'^2 + \varepsilon''^2}$.

Tridimensional variation with frequency and temperature of the real, M', and imaginary part of the modulus, M'', for PSFP, is shown in Fig. 11a, b. At lower frequencies, the real and imaginary parts of the modulus approaches zero, indicating that the electrode polarization phenomenon makes a negligible contribution; the long tail that appears is due to the large capacitance associated with the electrodes [51]. The presence of a peak in the imaginary modulus formalism at higher frequency indicates that ionic conduction is predominant in the structure of the studied polysulfone. As temperature increases, the peak maximum shifts to higher frequencies, which indicates that the conductivity of the charge carrier has been thermally activated.

AC-conductivity

Variation of conductivity, σ, with frequency at different temperatures is shown in Fig. 12. One can notice that the conductivity of many substances, especially of the amorphous ones (such as phosphorus-modified polysulfones), is governed by the $\sigma \propto f^n$ dependence. In this study, exponent n decreases with temperature increasing (according to Fig. 13), being within the $0.5 < n < 1$ limits, for a limited temperature domain (i.e., 0.4 and 50 °C). These n values characterize electronic conduction via a hopping process [52, 53]. Deviation from linearity at higher frequencies may be due to the dispersion of charge carriers produced by dipolar relaxation.

Generally, increasing temperature leads to an increase in electrical conductivity, with lower slope at high frequencies, for modified polysulfones. In this context, a model based on energy band gap representation could explain the temperature

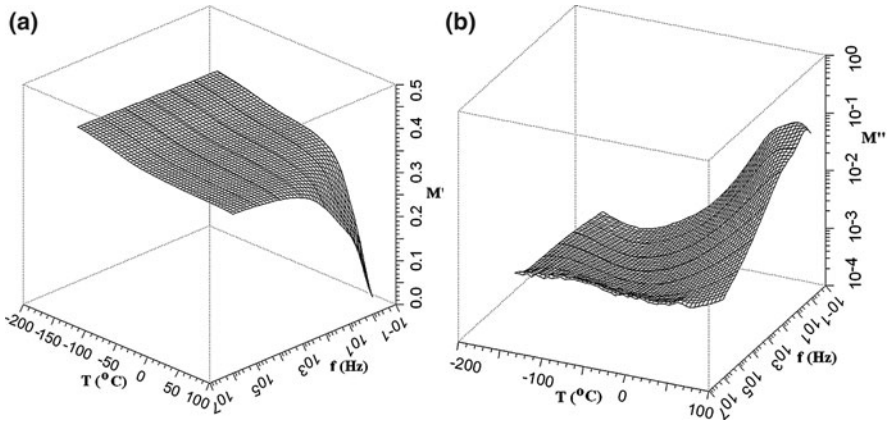

Fig. 11 Frequency and temperature dependencies of real part, M' (**a**) and imaginary part, M'' (**b**) of dielectric modulus for PSFP

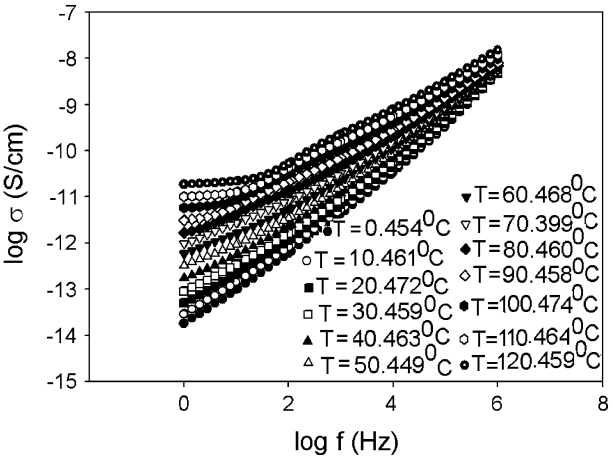

Fig. 12 Double logarithmic plot of electrical conductivity versus frequency at different temperatures, for PSFP

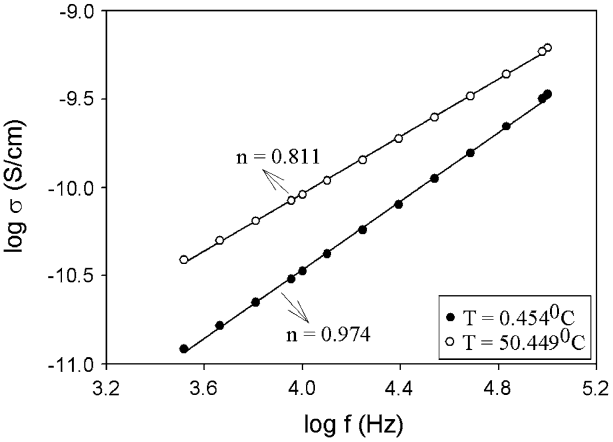

Fig. 13 Double logarithmic plot of electrical conductivity versus frequency at two temperatures, for PSFP

dependence on electrical conductivity. Electrical conductivity is not unilateral, because electronic conduction is accompanied by an ionic conduction—due to triphenylphosphonium pendant groups from the quaternized polysulfone (with 0.46 substitution degree). Plotting the relation between ln σ and $10^3/T$ (K^{-1}) shows a smaller slope over the lower temperature range (Fig. 14a), and a large slope over the higher temperature range (Fig. 14b) for PSFP. Moreover, at lower frequency, conductivity increases more rapidly with temperature than at higher frequency.

According to literature data [54], the higher slopes correspond to intrinsic electrical conduction, while slopes decrease at lower temperatures indicates a reduction in the impurity concentration of samples.

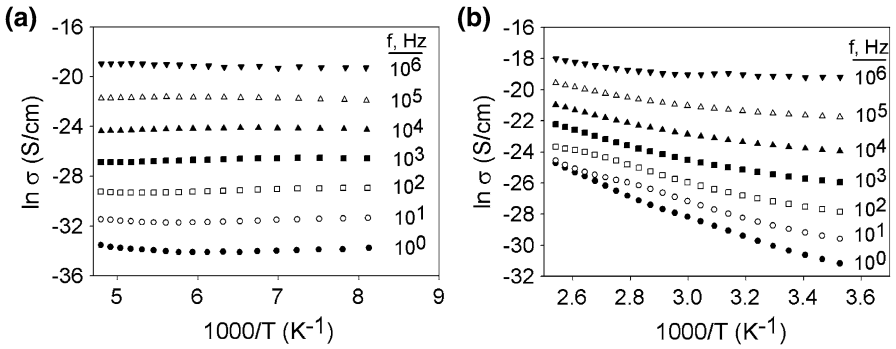

Fig. 14 Electrical conductivity versus temperature for PSFP in low (**a**) and high (**b**) temperature domains

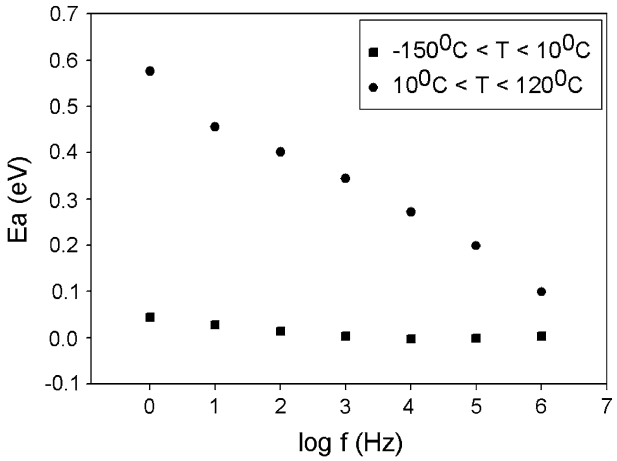

Fig. 15 Activation energy versus frequency at lower and higher temperature domains

The activation energies at different frequency values were calculated with Eq. 11 [55, 56]:

$$\sigma = \sigma_0 \exp(-\Delta E/kT) \tag{11}$$

where $\Delta E = E_G/2$ [57] denotes the thermal activation energy of electrical conduction, σ_0 is a parameter depending on the polymer nature, k is Boltzmann's constant ($k = 8.617343 \times 10^{-5}$ eV/K), and T represents the absolute temperature.

Figure 15 shows approximately the same values of activation energy for different frequency values over a lower temperature domain and a large variation with frequency at high temperatures. Consequently, electrical conductivity can be explained in terms of a band conduction mechanism, through band gap representation. Thus, the values of gap energy, $E_G = 2E_a$, ranged from 0.05 to 0.09 eV over the low-temperature domain, and the values of E_G ranged from 0.17 to 1.15 eV over the higher temperature domain, being attributed to the hopping processes characteristic to semiconductor materials.

The values of the thermal activation energy of electrical conduction are different from those obtained from the optical band gap energy presented in Table 2. Considering that light emission in the semiconductor is a creation process of photons, by annihilation of an electron–hole pair, the gap energy obtained from optical measurements should be higher than E_G from conductivity analysis. Furthermore, the differences between optical and electrical gap energy can be explained if assuming that the band gap optical energy of the system is related to the photon energy intensity of the photoluminescence spectra, and that band gap electrical energy is a consequence of the relaxation process appearing when temperature is modified.

Conclusions

This article evaluates the opto-electronic properties of a new quaternized polysulfone obtained by the quaternization reaction of chloromethylated polysulfone with triphenylphosphine. An extremely important roles in quaternized polysulfone applications is played by the control balance between the refractive indexes of the substructures, for obtaining the desired optical properties. Thus, knowledge on the optical properties prior to the preparation process is necessary. Theoretical evaluation of the refractive index shows that the ratio of molar refraction (proportional to the induced dipole moment) to molar volume for the different atoms present in the studied samples is reflected in the variation of the refractive index, and also that such values of the refractive index correspond to transparent materials. Also, theoretical data of the dielectric constants at visible wavelength (according to Maxwell law) confirm the lower polarizability of this sample.

On the other hand, quaternized polysulfone films appear as interesting materials, because of their transmittance properties:

- the films are transparent, with about 85% transmission over the whole visible spectral range. The transmission spectra start in the ultraviolet domain, being slightly different at higher wavelengths;
- the absorption edges of the investigated samples are similar to the typical edges for amorphous semiconductors, allowing the obtaining of optical parameters. The sample can be considered as a transparent material, with E_G values higher than 3.26 eV;
- the Urbach edge energy, E_U, which is related to the electric fields produced by charged impurities, and the Urbach tail energy, E_T, which characterizes the localized state induced by the polymer atomic structures, show the influence of the quaternized polysulfone side groups. Possible structural defects, such as break, abbreviation, or torsion of the polymer chains seem to be responsible for the low-energy absorption described by parameter E_T.

Dielectric spectroscopy measurements provided information on changes in the dielectric constant, dielectric loss and AC-conductivity for different frequencies and temperatures. Due to dielectric dispersion, the dielectric constant decreases with

increasing frequency. The dielectric loss behavior exhibits two types of relaxation, γ and β, relaxation γ being more visible. In the case of γ transition, a relatively broad distribution of the relaxation times and a symmetrical dielectric dispersion is evidenced.

The linear dependence of conductivity with frequency around room temperature is due to electronic conduction via a hopping process. Consequently, the electrical conductivity of studied sample can be explained in terms of band conduction mechanisms, through band gap representation. The values of thermal activation energy of electrical conduction are different from the results provided by absorption spectra, being first a consequence of the electronic transfer mechanism appearing when changing temperature, and, secondly, a consequence of the absorbed photons, electrons, and holes generators. In the same time, was observed that the presence of a peak in the imaginary part of electrical modulus at higher frequency indicates that ionic conduction is predominant in the structure of the studied polysulfone.

The findings of this study demonstrate that new quaternized polysulfones with triphenylphosphonium pendant group, with a suitable macromolecular design, may potentially offer important advantages for membrane applications.

References

1. Arthanareeswaran G, Mohan D, Raajenthiren M (2007) Preparation and performance of polysulfone-sulfonated poly(ether ether ketone) blend ultrafiltration membranes. Appl Surface Sci 253: 8705–8712. doi:10.1016/j.apsusc.2007.04.053
2. Lee ES, Hong SK, Kim YS, Lee JH, Won JC (2008) Preparation and characteristics of cross-linkable polysulfone having methylene methacrylate side-chain. J Appl Polym Sci 109:1–8. doi:10.1002/app.27944
3. Stamatialis DF, Papenburg BJ, Girones M, Saiful S, Bettahalli SNM, Schmitmeier S, Wessling M (2008) Medical applications of membranes: drug delivery, artificial organs and tissue engineering. J Membr Sci 308:1–34. doi:10.1016/j.memsci.2007.09.059
4. Yang MC, Lin WC (2003) Protein adsorbtion and platelet adhesion of polysulfone membrane immobilized with chitosan and heparin conjugate. Polym Adv Technol 14:103–113. doi:10.1002/pat.337
5. Raj SA, Rajesh S, Lakshmi K, Shobana KH, Mohan D (2010) Effect of functionalisation on polysulfone-based ultrafiltration membranes. Int J Nucl Desalin 4(1):18–27. doi:10.1504/IJND.2010.033763
6. Liu L, Chakma A, Feng X (2004) A new method of preparing ultrathin poly(ether block amide) membranes. J Membr Sci 235:43–52. doi:10.1016/j.memsci.2003.12.025
7. Summers GJ, Ndawuni MP, Summers CA (2003) Dipyridyl functionalized polysulfones for membrane production. J Membr Sci 226:21–33. doi:10.1016/j.memsci.2003.08.009
8. Wavhal DS, Fisher ER (2002) Hydrophilic modification of polyethersulfone membranes by low temperature plasma-induced graft polymerization. J Membr Sci 209:255–269. doi:10.1016/S0376-7388(02)00352-6
9. Song YQ, Sheng J, Wei M, Yuan XB (2000) Surface modification of polysulfone membranes by low-temperature plasma-graft poly(ethylene glycol) onto polysulfone membranes. J Appl Polym Sci 78:979–985. doi:10.1002/1097-4628(20001031)78:5<979:AID-APP60>3.0.CO;2-U
10. Blanco JF, Sublet J, Nguyen QT, Schaetzel P (2006) Formation and morphology studies of different polysulfones-based membranes made by wet phase inversion process. J Membr Sci 283:27–37. doi:10.1016/j.memsci.2006.06.011

11. Park JY, Acar MH, Akthakul A, Kuhlman W, Mayes AM (2006) Polysulfone-graft-poly(ethylene glycol) graft copolymers for surface modification of polysulfone membranes. Biomaterials 27: 856–865. doi:10.1016/j.biomaterials.2005.07.010
12. Hancock LF, Fagan SM, Ziolo MS (2000) Hydrophilic, semipermeable membranes fabricated with poly(ethylene oxide)-polysulfone block copolymer. Biomaterials 21:725–733. doi:10.1016/S0142-9612(99)00237-9
13. Shi Q, Su Y, Zhu S, Li C, Zhao Y, Jiang Z (2007) A facile method for synthesis of pegylated polyethersulfone and its application in fabrication of antifouling ultrafiltration membrane. J Membr Sci 303:204–212. doi:10.1016/j.memsci.2007.07.009
14. Higuchi A, Sugiyama K, Yoon BO, Sakurai M, Hara M, Sumita M, Sugawara S, Shirai T (2003) Serum protein adsorption and platelet adhesion on pluronic™-adsorbed polysulfone membranes. Biomaterials 24:3235–3245. doi:10.1016/S0142-9612(03)00186-8
15. Kim YW, Ahn WS, Kim JJ, Kim YH (2005) In situ fabrication of self-transformable and hydrophilic poly(ethylene glycol) derivative-modified polysulfone membranes. Biomaterials 26:2867–2875. doi:10.1016/j.biomaterials.2004.08.026
16. Sotiroiu K, Pispas S, Hadjichristidis N (2004) Effect of the end-positioning of a lithium sulfonate group on the aggregation and micellization behaviour of ω-lithium sulfonate polystyrene-block-polyisoprenes. Macromol Chem Phys 205:55–62. doi:10.1002/macp.200300049
17. Ismail AF, Hafiz WA (2002) Effect of polysulfone concentration on the performance of membrane-assisted lead acid battery. J Sci Technol 24(Suppl.):815–821. ISSN 0125-3395
18. Savariar S, Underwood GS, Dickinson EM, Schielke PJ, Hay AS (2002) Polysulfone with lower levels of cyclic dimer: use of MALDI-TOF in the study of cyclic oligomers. Desalination 144(1–3):15–20. doi:10.1016/S0011-9164(02)00282-5
19. Ydens I, Moins S, Degée P, Dubois P (2005) Solution properties of well-defined 2-(dimethylamino)ethyl methacrylate-based (co)polymers: a viscometric approach. Eur Polym J 41:1502–1509. doi:10.1016/j.eurpolymj.2005.02.002
20. Li L, Yan G, Wu J (2009) Modification of polysulfone membranes via surface-initiated atom transfer radical polymerization and their antifouling properties. J Appl Polym Sci 111:1942–1946. doi:10.1002/app.29204
21. Popa A, Ilia Gh, Davidescu CM, Iliescu S, Plesu N, Pascariu A, Zhang Z (2006) Wittig-Horner reactions on styrene-divinylbenzene supports with benzaldehyde side-groups. Polym Bull 57:189–197. doi:10.1007/s00289-006-0553-z
22. Popa A, Davidescu CM, Trif R, Ilia Gh, Iliescu S, Dehelean Gh (2003) Study of quaternary "onium" salts grafted on polymers: antibacterial activity of quaternary phosphonium salts grafted on "gel-type" styrene-divinylbenzene copolymers. React Funct Polym 55(2):151–158. doi:10.1016/S1381-5148(02)00224-9
23. Schuster M, Rager T, Noda A, Kreuer KD, Maier J (2005) About the choice of the protogenic group in PEM separator materials for intermediate temperature, low humidity operation: a critical comparison of sulfonic acid, phosphonic acid and imidazole functionalized model compounds. Fuel Cells 5(3):355–365. doi:10.1002/fuce.200400059
24. Kreuer KD (2002) On solids with liquid like properties and the challenge to develop new proton-conducting separator materials for intermediate-temperature fuel cells. ChemPhysChem 3(9):771–775. doi:10.1002/1439-7641(20020916)3:9<771:AID-CPHC771>3.0.CO;2-Y
25. Paddison SJ, Kreuer KD, Maier J (2006) About the choice of the protogenic group in polymer electrolyte membranes: ab initio modelling of sulfonic acid, phosphonic acid, and imidazole functionalized alkanes. Phys Chem Chem Phys 8:4530–4542. doi:10.1039/B611221H
26. Lafitte B, Jannasch P (2005) Phosphonation of polysulfones via lithiation and reaction with chlorophosphonic acid esters. J Polym Sci A 43:273–286. doi:10.1002/pola.20487
27. Petreus O, Avram E, Serbezeanu D (2010) Synthesis and characterization of phosphorus-containing polysulfone. Polym Eng Sci 50:48–56. doi:10.1002/pen.21508
28. Ioan S, Buruiana LI, Petreus O, Avram E, Stoica I, Ioanid GE (2011) Rheological and morphological properties of phosphorus-containing polysulfones. Polym Plast Technol Eng 50:36–46. doi:10.1080/03602559.2010.512346
29. Ioan S, Buruiana LI, Avram E, Petreus O, Musteata VE (2011) Optical, dielectric and conduction properties of new phosphorus-modified polysulfones. J Macromol Sci B 50:1571–1590. doi:10.1080/00222348.2010.541848
30. Lorenz L (1880) On the refraction constant. Wied Ann Phys 11:70–75

31. Lorentz HA (1880) On the relationship between the propagation of light and mass density. Wied Ann Phys 4:641–665
32. Davis EA, Mott NF (1970) Conduction in non-crystalline systems. V. Conductivity, optical absorption and photoconductivity in amorphous semiconductors. Philos Mag 22(179):903–922. doi:10.1080/14786437008221061
33. Tauc J, Menth A, Wood DL (1970) Optical and magnetic investigations of the localized states in semiconducting glasses. Phys Rev Lett 25:749–752. doi:10.1103/PhysRevLett.25.749
34. Tauc J, Menth A (1972) States in the gap. J Non-Cryst Solids 8–10:569–585. doi:10.1016/0022-3093(72)90194-9
35. Jarząbek B, Weszka J, Burian A, Pocztowski G (1996) Optical-properties of amorphous thin-films of the Zn-P system. Thin Solid Films 279:204–208. doi:10.1016/0040-6090(95)08162-3
36. Jarząbek B, Schab-Balcerzak E, Chamenko T, Sek D, Cisowski J, Volozhin A (2002) Optical properties of new aliphatic-aromatic co-polyimides. J Non-Cryst Solids 299–302:1057–1061. doi:10.1016/S0022-3093(01)01130-9
37. Jarząbek B, Weszka J, Domański M, Jurusik J, Cisowski J (2008) Optical studies of aromatic polyazomethine thin films. J Non-Cryst Solids 354:856–862. doi:10.1016/j.jnoncrysol.2007.08.013
38. Albu RM, Avram E, Musteata VE, Homocianu M, Ioan S (2011) Opto-electrical properties of some quaternized polysulfones. High Perform Polym 23(1):85–96. doi:10.1177/0954008310379166
39. Hougham G, Tesoro G, Viehbeck A, Chapple-Sokol D (1994) Polarization effects of fluorine on the relative permittivity in polyimides. Macromolecules 27:5964–5971. doi:10.1021/ma00099a006
40. Groh W, Zimmermann A (1991) What is the lowest refractive index of an organic polymer? Macromolecules 24(25):6660–6663. doi:10.1021/ma00025a016
41. Sayre R (1958) The extension of bond and molar refraction concepts to liquid organic phosphorus compounds. J Am Chem Soc 80(20):5438–5440. doi:10.1021/ja01553a030
42. Nada AMA, Dawy M, Salama AH (2004) Dielectric properties and ac-conductivity of cellulose polyethylene glycol blends. Mater Chem Phys 84:205–215. doi:10.1016/S0254-0584(02)00418-2
43. Saxena P, Gaur MS, Shukla P, Khare PK (2008) Relaxation investigation in polysulfone: thermally stimulated discharge current and dielectric spectroscopy. J Electrost 66:584–588. doi:10.1016/j.elstat.2008.07.002
44. Rudnik E, Dobkowski Z (1995) Investigations and molecular modeling of some thermophysical properties of polysulfones. J Therm Anal Calorim 45:1153–1158. doi:10.1007/BF02547488
45. Comer AC, Kalika DS, Rowe BW, Freeman BD, Paul DR (2009) Dynamic relaxation characteristics of Matrimid® polyimide. Polymer 50(3):891–897. doi:10.1016/j.polymer.2008.12.013
46. Starkweather HW (1981) Simple and complex relaxations. Macromolecules 14(5):1277–1281. doi:10.1021/ma50006a025
47. Starkweather HW (1991) Aspects of simple, non-cooperative relaxations. Polymer 32:2443–2448. doi:10.1016/0032-3861(91)90087-Y
48. Zhang S, Runt J (2004) Segmental dynamics and ionic conduction in poly(vinyl methyl ether)-lithium perchlorate complexes. J Phys Chem B 108(20):6295–6302. doi:10.1021/jp0499777
49. Havriliak S, Havriliak SJ (1997) Dielectric and mechanical relaxation in materials. Hanser Publishers, Cincinnati
50. Pradhan DK, Choudhary RNP, Samantaray BK (2008) Studies of structural, thermal and electrical behaviour of polymer nanocomposite electrolytes. eXPRESS Polym Lett 2(9):630–638. doi:10.3144/expresspolymlett.2008.76
51. Nithya H, Selvasekarapandian S, Kumar DA, Sakunthala A, Hema M, Christopherselvin P, Kawamura J, Baskaran R, Sanjeeviraja C (2011) Thermal and dielectric studies of polymer electrolyte based on P(ECH-EO). Mater Chem Phys 126:404–408. doi:10.1016/j.matchemphys.2010.10.047
52. Kuczkowski A, Zielinski R (1982) The AC conductivity of the polyvinylcarbazole-tetracyanoquinodimethane (PVK:TCNQ) CT complex. J Phys D Appl Phys 15(9):1765–1768. doi:10.1088/0022-3727/15/9/021
53. Clarke PJ, Ray AK, Tsibouklis J, Werninck AR (1991) Dielectric loss in novel disubstituted polydiacetylenes. J Mater Sci: Mater Electronics 2(1):18–20. doi:10.1007/BF00694999
54. Smith R (1980) Semiconductors. Cambridge University Press, London
55. Muruganand S, Narayandass SK, Mangalaraj D, Vijayan TM (2001) Dielectric and conduction properties of pure polyimide films. Polym Int 50:1089–1094. doi:10.1002/pi.749
56. Banik I (2009) One way to explain the Meyer-Neldel rule. Chalcogenide Lett 6(12):629–633. ISSN: 15848663
57. Meier H (1974) Organic semiconductors. Verlag Chemie, Weinheim